

Structure of excited vortices with higher angular momentum in Bose-Einstein condensates

Jian-Ming Tang

Department of Physics and Astronomy, University of Iowa, Iowa City, Iowa 52242-1479, USA

(Received 1 October 2003; published 25 October 2004)

The structure of vortices in Bose-Einstein condensed atomic gases is studied taking into account many-body correlation effects. It is shown that for excited vortices the particle density in the vortex core increases as the angular momentum of the system increases. The core density can increase by several times with only a few percent change in the angular momentum. This result provides an explanation for the observations in which the measured angular momentum is higher than the estimation based on counting the number of vortices and the visibility of the vortex cores is simultaneously reduced. The calculated density profiles for the excited vortices are in good agreement with experimental measurements of a single vortex.

DOI: 10.1103/PhysRevA.70.043626

PACS number(s): 03.75.Lm, 03.75.Hh, 03.75.Kk, 67.40.Vs

When a superfluid is put into rotation, vorticity is split into discrete vortex lines rather than continuously distributed as in the case of solid-body rotation [1,2]. The dynamics, such as formation, reconnection, and decay, of vortex lines is influenced by the microscopic structure of the vortex core [3]. Direct imaging of rotating Bose-Einstein condensed atomic gases (BEC's) has revealed, for the first time, the particle density profile of the vortex core in neutral superfluids [4–8]. The particle density is reduced in the core, and the density dips in the measured images are used to identify the presence of vortex lines in the experiments. In the mean-field approximation, known as the Gross-Pitaevskii (GP) theory [9,10], the predicted particle density at the center of the vortex core is exactly zero because the phase of the single-particle wave function at the vortex line is not well defined. Observationally, the particle density at the core center is finite and varies in a wide range with different experimental conditions. The finite core density in the observations could arise due to the finite resolution of the imaging systems. However, in many cases the core densities appear to be quite large and not simply an experimental artifact.

Theoretically, finite particle density at the core center results from quantum fluctuations of the locations of vortex lines due to many-body correlations [11–13]. The estimated density at the core center for a straight vortex line after taking into account quantum fluctuations is comparable to the density of particles depleted from the condensate in the ground state of a BEC [11], which is not sufficient to explain the observed large core densities. The fact that the core density is large and varies from measurements to measurements suggests that these vortex lines may be in different vibrating modes [14] rather than straight. In this paper, the structure of excited vortices is studied using many-body wave functions that incorporate quantized motion of the vortex lines. It is proposed that the observed vortices with large core densities are in vibrating modes corresponding to excited rotational states of BEC's with an angular momentum higher than the stationary GP states. This proposal is based on my results that the core density increases rapidly as the angular momentum increases and is supported by the experimental findings that the angular momentum per particle, averaged over an ensemble of one-vortex systems, is larger than \hbar [15,16]. The calculated density profiles for the excited vortices are in

good agreement with experimental measurements of a single vortex in the center of the trap. The existence of vortices with a higher angular momentum also provides a possible explanation for the observations in which the measured angular momentum is higher than the estimation based on counting the number of vortices, and the visibility of the vortex cores is simultaneously reduced [17]. Note that for the observations reported in Ref. [17], the visibility of the vortex cores is also reduced due to a static distortion of the trap and bending for off-centered vortices. The present theory only considers a single vortex in the center of the trap and does not take into account nonequilibrium processes during the formation of vortex lattices.

The importance of many-body correlations in the vortex core can be seen in the following way. In the GP theory, the description of a vortex line is “classical” in the sense that the position and velocity of a vortex line can be simultaneously determined. A quantum description would be required if the position uncertainty of a vortex line is comparable to the size of the vortex core. The position uncertainty of a vortex line is given by the interatomic spacing [13,18], because the total angular momentum of the system would be altered by one \hbar if a vortex line fluctuates across an atom in the superfluid. The size of the vortex core is given by the healing length which is determined through a balance between the kinetic and potential energies for a density gradient. Although the healing length can be much larger than the interatomic spacing in the weakly interacting limit, they are often comparable with each other in realistic situations (see Table I for comparisons). As a result, the quantum fluctuations of vortex lines are generally important. We should note that although it is possible to address the finite column densities within the framework of the GP theory by considering bent vortex lines [19], such considerations are limited to metastable states with broken rotational symmetry and a lower angular momentum.

For simplicity I consider a rotating BEC with only a single vortex point in two dimensions, but the formulation can be applied to a vortex line in a three-dimensional system. To obtain a quantum description for the vortex, many-body wave functions are constructed as linear combinations of the GP wave functions parameterized by the location of the vortex [13,18]. The GP wave functions are used as basis states

TABLE I. Ratios between the interatomic spacing σ and the healing length ξ at the center of the traps in different experiments. In the Thomas-Fermi approximation, the ratio is given by $\sigma/\xi = 2(15\pi^5 N m^3 a_s^6 \omega_\perp^2 \omega_\parallel / \hbar^3)^{1/15}$, where N is the total number of particles, m is the mass, a_s is the s -wave scattering length, and ω_\perp and ω_\parallel are the trapping frequencies in the perpendicular and parallel directions to the rotation axis. The last column shows the ratio for liquid helium assuming that the vortex core radius is 1 Å.

Atoms	⁸⁷ Rb [4]	⁸⁷ Rb [5]	²³ Na [6]	⁸⁷ Rb [7]	⁸⁷ Rb [8]	⁴ He
$\omega_\perp/2\pi$ (Hz)	7.8	219	84	62	8.35	
$\omega_\parallel/2\pi$ (Hz)	7.8	11.7	20	175	5.45	
N	3×10^5	10^5	5×10^7	2×10^4	10^6	
σ/ξ	0.6	0.9	0.9	0.8	0.6	3.5

analogous to the position space representation of a particle in quantum mechanics. For a N -particle system, such a wave function is written as,

$$\Psi(\mathbf{r}_1, \dots, \mathbf{r}_N) = \int d^2\mathbf{r}_0 F(\mathbf{r}_0) \prod_{i=1}^N \psi_{\text{GP}}(\mathbf{r}_i; \mathbf{r}_0), \quad (1)$$

where $F(\mathbf{r}_0)$ is the weight function that represents the effective dynamics of the vortex and $\psi_{\text{GP}}(\mathbf{r}; \mathbf{r}_0)$ is the normalized solution of the time-independent GP equation with a vortex located at $\mathbf{r}_0=(r_0, \theta_0)$. When Eq. (1) is generalized to describe a vortex line in three dimensions, the weight function becomes an effective ‘‘wave function’’ of a string rather than a particle. For the case of a straight vortex line with the zero-point motion, the wave function in Eq. (1) is similar to the shadow wave functions used to study vortices in liquid ⁴He [20].

The weight functions for the energy eigenstates of the vortex can be solved by diagonalizing the many-body Hamiltonian within the sub-Hilbert space spanned by the GP basis states. In the case that the system has a uniform ground state with a density $\rho_{2D}=\sigma^{-2}$, the weight functions are found [13] to be

$$F_{n,l}(\mathbf{r}_0) = \mathcal{N}_{n,l} x^{|l|} e^{-x^2/2} e^{il\theta_0} {}_1F_1(a, b; x^2), \quad (2)$$

where $n \geq 0$, $n \geq l \geq -N$, $x = \sqrt{\pi} r_0 / \sigma$, $\mathcal{N}_{n,l}$ is the normalization constant determined by $\langle \Psi_{n,l} | \Psi_{n,l} \rangle = 1$, $a = -(2n - l - |l|) / 2$, $b = |l| + 1$, and ${}_1F_1(a, b; x^2)$ is the confluent hypergeometric function [21]. It is straightforward to verify that the state $|\Psi_{n,l}\rangle$ is an eigenstate of the angular momentum operator L_z with eigenvalue $(N+l)\hbar$, given that the phase of $\psi_{\text{GP}}(\mathbf{r}; \mathbf{r}_0)$ takes the form of $\theta + f(\theta - \theta_0)$ in azimuthally symmetric systems. For example, the weight function $F_{0,0}(\mathbf{r}_0)$ is a Gaussian centered at the origin, and the state $|\Psi_{0,0}\rangle$ is the corresponding many-body state that includes the zero-point motion to the Hartree state of a centered vortex. The weight functions in Eq. (2) have exactly the same form as the energy eigenfunctions of a charged particle in a constant magnetic field [22]. This is because the motion of a vortex is also driven by a velocity-dependent transverse force like the Lorentz force. For nonuniform systems such as BEC’s in harmonic traps, the exact solutions for the weight functions are not known.

However, in the case that the radius of the system is much larger than the size of the vortex core and the vortex is near the trap center, the weight functions can be approximated by Eq. (2) with ρ_{2D} equal to the local density of the ground state [13]. Therefore, I will use the wave function in Eq. (1) with the weight functions given by Eq. (2) to study the structure of vortex cores in trapped BEC’s.

To use Eq. (1), the first step is to set up the GP basis states. In order to solve the GP equation for a system with a given number of particles, it is convenient to choose the length unit to be the healing length $\xi = \sqrt{\sigma^3 / 8\pi a_s}$, where σ is the interatomic spacing of the ground state at the trap center and a_s is the s -wave scattering length characterizing the interaction strength between particles. The ground-state wave function $\bar{\psi}_{\text{gs}}(r)$ is first solved with the boundary condition $\bar{\psi}_{\text{gs}}(0)=1$. This particular choice of boundary condition and length unit has the advantage that the normalization of the wave function is related to the total number of particles as

$$N = \frac{1}{\sigma^2} \int d^2\mathbf{r} |\bar{\psi}_{\text{gs}}(r)|^2. \quad (3)$$

Then the GP state that has a centered vortex and the same number of particles is solved and written as

$$\bar{\psi}_{\text{GP}}(\mathbf{r}; 0) = g(r) \bar{\psi}_{\text{gs}}(r) e^{i\theta}, \quad (4)$$

where $g(r)$ is the amplitude ratio of the vortex state to the ground state. The normalized GP basis states with an off-centered vortex can now be approximated by

$$\psi_{\text{GP}}(\mathbf{r}; \mathbf{r}_0) \approx \frac{1}{\sqrt{N}\sigma} g(|\mathbf{r} - \mathbf{r}_0|) \bar{\psi}_{\text{gs}}(r) e^{i\phi(\mathbf{r}; \mathbf{r}_0)}, \quad (5)$$

where the phase satisfies the following set of linear differential equations:

$$\nabla \times \nabla \phi(\mathbf{r}; \mathbf{r}_0) = 2\pi \delta(\mathbf{r} - \mathbf{r}_0), \quad (6)$$

$$\nabla \cdot [|\psi_{\text{GP}}(\mathbf{r}; \mathbf{r}_0)|^2 \nabla \phi(\mathbf{r}; \mathbf{r}_0)] = 0. \quad (7)$$

The first equation specifies that the vortex is located at \mathbf{r}_0 , and the second is the continuity equation which directly follows from the GP equation. The general solutions of Eq. (6) can be written as $\phi(\mathbf{r}; \mathbf{r}_0) = \vartheta(\mathbf{r} - \mathbf{r}_0) + \tilde{\phi}(\mathbf{r}; \mathbf{r}_0)$, where $\vartheta(\mathbf{r} - \mathbf{r}_0)$ is the azimuthal angle of the vector $\mathbf{r} - \mathbf{r}_0$ and $\tilde{\phi}(\mathbf{r}; \mathbf{r}_0)$ is a single-valued function that remains to be determined by Eq. (7).

In the case that the vortex is close to the trap center, the correction term $\tilde{\phi}(\mathbf{r}; \mathbf{r}_0)$ is only significant in the region, $r > r_0$. In this region, the general solution of Eq. (6) can be expanded as a Fourier series,

$$\phi(\mathbf{r}; \mathbf{r}_0) = \theta + \sum_{j=1}^{\infty} \left(\frac{r_0}{r}\right)^j \left[\tilde{\phi}_j(r) + \frac{1}{j} \right] \sin[j(\theta - \theta_0)], \quad (8)$$

where the factor $1/j$ comes from the expansion of the azimuthal angle $\vartheta(\mathbf{r} - \mathbf{r}_0)$. Since the density profile of the vortex state in this region is not far from the ground-state density profile, we can replace $|\psi_{\text{GP}}(\mathbf{r}; \mathbf{r}_0)|^2$ in Eq. (7) with the den-

sity profile of the ground state, $\rho_0(r)=|\psi_{\text{gs}}(r)|^2$. By substituting Eq. (8) into Eq. (7), the differential equation for each $\tilde{\phi}_j(r)$ is obtained as follows:

$$\left[\frac{1}{r} \frac{d}{dr} r \frac{d}{dr} + \frac{\rho'_0(r)}{\rho_0(r)} \frac{d}{dr} - \frac{j^2}{r^2} \right] \frac{\tilde{\phi}_j(r)}{r^j} = \frac{1}{r^{j+1}} \frac{\rho'_0(r)}{\rho_0(r)}, \quad (9)$$

where $\rho'_0(r)=d\rho_0(r)/dr$. To solve Eq. (9), two boundary conditions are needed. The boundary condition at a distance far away from the trap center can be obtained by noting that $\rho_0(r)$ behaves like a Gaussian at large distances, and, therefore,

$$\lim_{r \rightarrow \infty} \frac{\rho'_0(r)}{\rho_0(r)} = -\infty. \quad (10)$$

Thus, the asymptotic value of the first derivative of the solution is fixed by

$$\frac{d}{dr} \left[\frac{\tilde{\phi}_j(r)}{r^j} \right] \sim \frac{1}{r^{j+1}} \quad \text{for } r \rightarrow \infty. \quad (11)$$

The other boundary condition can be chosen as $\tilde{\phi}_j(0)=0$ because the correction near the origin is small in a large system. With these two boundary conditions, Eq. (9) is solved numerically to obtain $\tilde{\phi}_j(r)$ and, thus, the GP basis states.

The second step is to find the overlap between two GP basis states because they are not orthogonal to each other. However, it is sufficient to calculate the overlap between two single-particle wave functions up to the second order in the separation between their vortex coordinates because the corresponding many-body wave functions are nearly orthogonal. The overlap between two single-particle wave functions is

$$\begin{aligned} \langle \psi_{\text{GP}}(\mathbf{r}'_0) | \psi_{\text{GP}}(\mathbf{r}_0) \rangle &\approx \int d^2\mathbf{r} e^{i[\phi(\mathbf{r};\mathbf{r}_0)-\phi(\mathbf{r};\mathbf{r}'_0)]} g(|\mathbf{r}-\mathbf{r}'_0|) \\ &\quad \times g(|\mathbf{r}-\mathbf{r}_0|) |\psi_{\text{gs}}(r)|^2 \\ &\approx \int d^2\mathbf{r} e^{i[\vartheta(\mathbf{r};\mathbf{r}_0)-\vartheta(\mathbf{r};\mathbf{r}'_0)]} g(|\mathbf{r}-\mathbf{r}'_0|) \\ &\quad \times g(|\mathbf{r}-\mathbf{r}_0|) |\psi_{\text{gs}}(r)|^2 - |\mathbf{r}_0-\mathbf{r}'_0|^2 \\ &\quad \times \int \frac{d^2\mathbf{r}}{4r^2} [2\tilde{\phi}_1(r) + \tilde{\phi}_1(r)^2] |\psi_{\text{GP}}(\mathbf{r};0)|^2 \\ &\approx 1 - \alpha_R \frac{|\mathbf{r}_0-\mathbf{r}'_0|^2}{N\sigma^2} - i\alpha_I \frac{\hat{\mathbf{z}} \cdot \mathbf{r}_0 \times \mathbf{r}'_0}{N\sigma^2}, \quad (12) \end{aligned}$$

where α_R and α_I are numerical constants for a given system. The coefficient α_R generally scales logarithmically with the system size, while the coefficient α_I is not sensitive to the system size or local density variations and is exactly given by π in an asymptotically uniform system [13].

Finally, the density profile of the state $|\Psi_{n,l}\rangle$ is given by

$$\begin{aligned} \rho_{n,l}(\mathbf{r}) &= N \int d^2\mathbf{r}'_0 \int d^2\mathbf{r}_0 F_{n,l}^*(\mathbf{r}'_0) F_{n,l}(\mathbf{r}_0) \psi_{\text{GP}}^*(\mathbf{r};\mathbf{r}'_0) \psi_{\text{GP}}(\mathbf{r};\mathbf{r}_0) \\ &\quad \times \exp \left[-\alpha_R \frac{|\mathbf{r}'_0-\mathbf{r}_0|^2}{\sigma^2} - i\alpha_I \frac{\hat{\mathbf{z}} \cdot \mathbf{r}_0 \times \mathbf{r}'_0}{\sigma^2} \right], \quad (13) \end{aligned}$$

where the many-body overlap corresponding to the single-particle overlap in Eq. (12) falls off exponentially with the separation of the vortex coordinates in the large- N limit. To compare this two-dimensional theory with experimental data, we assume that the healing length ξ and the interatomic spacing σ at the trap center are the same as in the three-dimensional (3D) system. In the following, I will use the experimental conditions of Madison *et al.* [5] (the trapping frequencies are listed in Table I). For a BEC with $N_{3\text{D}}=1.4 \times 10^5$ particles, the healing length is $\xi=0.19 \mu\text{m}$ and the interatomic spacing is $\sigma=0.17 \mu\text{m}$. The corresponding number of particles in two dimensions given by Eq. (3) is about 350. The two coefficients in the overlap are $\alpha_R=5.84$ and $\alpha_I=3.25$.

Although all states described by Eq. (2) can exist, some of them are more stable and likely to be realized in actual experiments than the others. A rotating BEC is typically created by a stirring laser beam. The system is first driven by the laser stirrer for a period of time and then relaxes to a stationary state. The laser stirrer breaks the rotational symmetry and transfers both energy and angular momentum into the system. During the relaxation period, the energy can relax through collisional processes, but it is harder for the angular momentum to relax unless the rotational symmetry is broken by other means. There is experimental evidence showing that the system can maintain its angular momentum for a long period of time [23]. This leads us to assume that the system will fall into the lowest-energy state with the initially given angular momentum. As the angular momentum of the system increases, more and more vortices will form. However, it is energetically favorable to excite the existing vortices if the change in angular momentum is small. The energy cost for introducing an additional vortex into the system is approximately $\ln(R/\xi)\pi\hbar^2/m\sigma^2$, where R is the characteristic radius of the system, while the energy cost for having an excited vortex is approximately $\beta n\pi\hbar^2/m\sigma^2$ [13,18], where β is an umerical constant less than 1 and n is the angular momentum increase. Although adding another vortex would eventually become energetically favorable for larger values of the angular momentum, the critical value (n_c) is so far not known. If we consider a two-dimensional system with parameters similar to those in Ref. [5] ($R/\xi \approx 15$), but the ground state density is constant, then β is about 0.05 and $n_c \approx 50$ [13]. Accurate comparison of the energies of different vortex configurations is complicated by the nonuniformity of the system and require further studies.

In the case of a single excited vortex, the lowest-energy state for a given angular momentum is the $|\Psi_{n,n}\rangle$ state. Hence the density profiles of the $|\Psi_{n,n}\rangle$ states are compared against experimental data. Figure 1(a) shows that the data of Madison *et al.* [5] can be best fitted with the state that the angular momentum is increased by 5% ($n=18$ compared to $N=350$). The experimental data are shown by the solid dots.

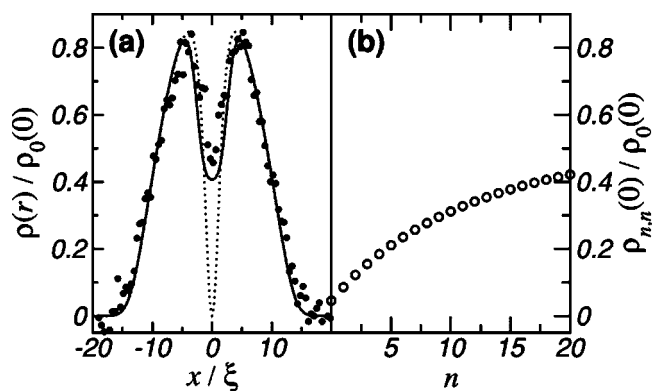


FIG. 1. (a) The integrated column density profile of a rotating BEC with a vortex at the center. The solid dots show the experimental data in Ref. [5]. The solid line shows the density profile of the excited state ($n=18$) whose angular momentum per particle is about $1.05\hbar$. The 3D column density is approximated by using the 2D results as $\rho_{\text{col}}(r)=\rho_{2\text{D}}(r)\bar{\psi}_{\text{gs}}(r)$. The density profile of the GP state is shown as the dotted line for comparison. $\rho_0(0)$ is the central density of the ground state. (b) The open circles show the scaling behavior of the central density with respect to the angular momentum increase.

Only one centered vortex core is clearly visible, and the core density profile is significantly deviated from the density pro-

file of the GP state ($L_z=N\hbar$). The value $n=18$ should only be considered as an upper bound of the angular momentum increase for this particular data set since the measured core density was partly contributed by the finite resolution of the imaging system. Figure 1(b) shows the calculated trend that the core density increases with increasing angular momentum of the system ($L_z=(N+n)\hbar$).

In summary, I have calculated the density profiles of different rotational states of a trapped Bose gas with one quantized vortex using many-body wave functions which are linear combinations of GP wave functions. The core density increases with increasing angular momentum of the system, which suggests that vortices with large core densities are in excited states with higher angular momentum. The possibility of having excited vortices suggests that for given angular momentum, the lower-energy rotational state can have number of vortices less than expected in the mean-field theory. From the quantitative agreement on the density profile between the theoretical prediction and the experimental measurements, it is suggested that the rotating Bose gas observed experimentally by Madison *et al.* [5] is in a state with angular momentum higher than one \hbar per atom.

The author thanks D. J. Thouless and A. Bulgac for valuable discussions and K. W. Madison and J. Dalibard for providing data shown in Fig. 1.

[1] L. Onsager, *Nuovo Cimento, Suppl.* **6**, 249 (1949).
 [2] R. P. Feynman, in *Progress in Low Temperature Physics*, edited by C. J. Gorter (Elsevier Science Publishers B.V., Amsterdam, 1955), Vol. 1, Chap. 2, pp. 17–53.
 [3] R. J. Donnelly, *Quantized Vortices in Helium II* (Cambridge University Press, New York, 1991).
 [4] M. R. Matthews *et al.*, *Phys. Rev. Lett.* **83**, 2498 (1999).
 [5] K. W. Madison *et al.*, *Phys. Rev. Lett.* **84**, 806 (2000).
 [6] J. R. Abo-Shaeer *et al.*, *Science* **292**, 476 (2001).
 [7] E. Hodby *et al.*, *Phys. Rev. Lett.* **88**, 010405 (2001).
 [8] P. Engels *et al.*, *Phys. Rev. Lett.* **89**, 100403 (2002).
 [9] E. P. Gross, *Nuovo Cimento* **20**, 454 (1961).
 [10] L. P. Pitaevskii, *Zh. Eksp. Teor. Fiz.* **40**, 646 (1961) [*Sov. Phys. JETP* **13**, 451 (1961)].
 [11] A. L. Fetter, *Phys. Rev. Lett.* **27**, 986 (1971); *Ann. Phys. (N.Y.)* **70**, 67 (1972).
 [12] J.-M. Tang, *J. Low Temp. Phys.* **121**, 287 (2000).
 [13] J.-M. Tang, Ph.D. thesis, University of Washington, 2001.
 [14] Sir W. Thomson, *Philos. Mag.* **10**, 155 (1880).
 [15] F. Chevy, K. W. Madison, and J. Dalibard, *Phys. Rev. Lett.* **85**, 2223 (2000).
 [16] E. Hodby *et al.*, *Phys. Rev. Lett.* **91**, 090403 (2003).
 [17] V. Bretin *et al.*, *Phys. Rev. Lett.* **92**, 050403 (2004).
 [18] J.-M. Tang, *Int. J. Mod. Phys. B* **15**, 1601 (2001).
 [19] J. J. García-Ripoll and V. M. Pérez-García, *Phys. Rev. A* **63**, 041603(R) (2001); **64**, 053611 (2001).
 [20] M. Sadd, G. V. Chester, and L. Reatto, *Phys. Rev. Lett.* **79**, 2490 (1997).
 [21] *Handbook of Mathematical Functions, with Formulas, Graphs, and Mathematical Tables*, edited by M. Abramowitz and I. A. Stegun (Dover, New York, 1977).
 [22] L. D. Landau and E. M. Lifshitz, *Quantum Mechanics: Non-Relativistic Theory*, 3rd ed. (Pergamon, Oxford, 1977).
 [23] V. Bretin, P. Rosenbusch, and J. Dalibard, *J. Opt. B: Quantum Semiclassical Opt.* **5**, S23 (2003).